ENGINEERING MATHEMATICS
AND COMPUTING LAB

UNIVERSITÄT
HEIDELBERG
ZUKUNFT
SEIT 1386

Sparse Grids for quantifying motion uncertainties in biomechanical models of radiotherapy patients

Chen Song, Markus Stoll, Kristina Giske, Rolf Bendl, Vincent Heuveline

Preprint No. 2017-01

Preprint Series of the Engineering Mathematics and Computing Lab (EMCL)

http://emcl.iwr.uni-heidelberg.de

Preprint Series of the Engineering Mathematics and Computing Lab (EMCL)
ISSN 2191–0693
Preprint No. 2017-01

Affiliation of the Authors

Chen Song[a,b,1], Markus Stoll[c,d], Kristina Giske[c,d], Rolf Bendl[c,d], Vincent Heuveline[a,b]

[a] *Engineering Mathematics and Computing Lab (EMCL), Interdisciplinary Center for Scientific Computing (IWR), Heidelberg University, Germany*
[b] *HITS gGmbH, Heidelberg Institute for Theoretical Studies*
[c] *Department of Medical Physics in Radiation Oncology, German Cancer Research Center (DKFZ), Heidelberg, Germany*
[d] *Heidelberg Institute for Radiation Oncology (HIRO), National Center for Radiation Research in Oncology, Heidelberg, Germany*
[1] *Corresponding Author: Chen Song, chen.song@h-its.org*

Impressum

Heidelberg University
Interdisciplinary Center for Scientific Computing (IWR)
Engineering Mathematics and Computing Lab (EMCL)

Im Neuenheimer Feld 205,
69120 Heidelberg
Germany

Sparse Grids for quantifying motion uncertainties in biomechanical models of radiotherapy patients

Chen Song, Markus Stoll, Kristina Giske, Rolf Bendl, Vincent Heuveline

January 31, 2017

Abstract

Quantifying the uncertainties in biomedical simulations has strong potential in medical software systems. It allows us to improve objective confidence levels for numerical predictions. The Stochastic Collocation (SC) method is a promising way to create the link between existing simulation codes and advanced Uncertainty Quantification (UQ) methods, as it does not require modifying the original source code and meanwhile has better convergence rate comparing with traditional stochastic approaches.

We describe the implementation of the Stochastic Collocation method with an adaptive sparse grid numerical integration, and apply it in the context of radiotherapy treatment planning of patients with head and neck cancer. In this case, the statistical sampling of most probable postures of patient specific anatomy of the neck region is used to estimate deformations of the tumor region in order to find a suitable safety margin around target volumes.

Especially, in highly flexible body areas, like the neck and upper thorax regions, the number of degrees of freedom of motion patterns can be quite large. The fast and stable prediction of most probable motion patterns, derived from previous cohorts, influences the ability to incorporate uncertainties caused by motion into the treatment planning process. The optimal number of samples not only reduces the number of simulations needed to generate an individually fitted internal target volume as a starting point for a standardized planning target volume, but also promises to minimize computational demands in robust planning scenarios, where plans are challenged by different possible motion scenarios.

1 Introduction

Mathematical and numerical models are nowadays widely used in medical engineering; it provides important information for medical therapies or operations. Despite the patient-specific simulation played already a crucial role in increasing the quality of simulation results, but the uncertain source within the numerical model, which cannot be covered by deterministic simulation, could have huge influence on the numerical solutions, it might lead to an inaccurate surgical decision. Therefore, using an efficient method for quantifying the uncertainties for biomedical models and simulations becomes a real piratical question.

1.1 Sparse Grid technique

In general, there are mainly two kinds of uncertainties: **aleatoric** and **epistemic**. The aleatoric uncertainty (also referred to irreducible uncertainty) is the natural randomness in the physical process, e.g. experimental measure of a Young's modulus for a material. It could be improved by employing new technologies, whereas it cannot be eliminated. The epistemic uncertainty (also referred to reducible uncertainty) is due to the lack of knowledge, e.g. the assumption of boundary condition for flow computation. It can be reduced for example by using advanced mathematical models.

Unlike the intrusive methods [13], which requires a lot of efforts to modify and adapt the original implementation. The non-intrusive method performs essentially like an "outer loop", which could deploy directly the existing code. Besides, the non-intrusive methods are inherently suitable for parallel computing due to the independence of the computed realizations. There is a wide variety of non-intrusive methods, such as Monte-Carlo, non-intrusive Polynomial Chaos (NIPC) [16] [9] , Stochastic Collocation (SC) [14], Gaussian process regression, etc. The Stochastic Collocation method is flexible and performs favorable efficiency regarding to Monte-Carlo Method, but due to the multivariate integration process, the Stochastic Collocation methods is often limited by the "curse of dimensionality" [7]. However, the Sparse Grid (SG) technique, which is based on Smolyak's construction [20], could overcome this difficulty assuming certain conditions, with the result that the computational effort does not grow exponentially with respect to the dimension of uncertain parameters.

1.2 Motion uncertainties in radiotherapy

Head and neck cancer are currently treated with radiation therapy often combined with other treatment modalities [18]. The clinical target volume (CTV) for the curative treatment can be the primary tumor and surrounding volumes including the lymph nodes. Organs at risk (OARs) like brainstem or spinal cord tolerating only an organ-specific low exposure, are located in the vicinity of the CTV and thus define the desired location steepness of the gradients in the dose distribution.

Sophisticated techniques like Intensity Modulated Radiation Therapy (IMRT) allow to highly conform the high dose region to the CTV and limit the dose to surrounding tissue. Thus, each patient receives an individually optimized treatment plan. The treatment plan is generated based on a CT image of the patient. All CTVs and OARs are delineated and dose constraints for CTVs and OARs are predefined. Plan parameters are optimized by an inverse planning process to fulfill dose constraints. Details of the planning process can be found in [19] [2].

A daily image based patient setup (image guided radiation therapy, IGRT) in the treatment room (before each treatment fraction) is required to accurately place the patient on the treatment couch with respect to the treatment machine in order to take advantage of the precise planning [8]. While IGRT can compensate for rigid setup uncertainties with couch shifts (or rotations), remaining anatomical deformation cannot be corrected.

Due to deformations of the head and neck region during the treatment course, uncertainties in the administered accumulated dose distribution are introduced. A safety margin around the target volumes is introduced to guarantee the CTV coverage, but in the same time it can jeopardize the thresholds of the dose exposure in the OARs. There are different ways of margin generation in therapy planning, e.g. adding a constant isotropic 3 mm margin [4].

Isotropic margins do not cover complex deformation patterns of the head and neck region. The margin might be chosen unnecessary large in regions of small deformations and not large enough in regions with large deformations [26] [21]. The application of patient-specific biomechanical simulations allows to estimate an adjusted margin [21]. Therefore a large number of random deformation scenarios is simulated, the target region is transformed for each scenario and the results are super-imposed to build a margin covering (almost) all deformation scenarios. A large drawback of this method is the huge number of scenarios needed for the calculation. We will use Sparse grid techniques to reduce the number of samples.

1.3 Outline

This paper is structured in the following way: we start with the mathematical background related to Stochastic Collocation method and Sparse Grid integration in Section 2 as well as the medical background. Then a deformation model of the head and neck region based on mechanical elasticity theory is explained in Section 3. In Section 4, We compare Sparse Grid and Monte-Carlo method by using an analytical calculated reference solution in a simple elastic beam simulation with random boundary conditions to validate our Sparse Grid Implementation. Afterwards, we continue this comparison for an ITV-to-CTV margin generation for head and neck cancer patients. Section 5 concludes this paper.

2 Mathematical background

In this section, we give some basic concepts about the Stochastic Collocation method and the Sparse Grid sampling technique.

Before introducing the Stochastic Collocation method, we need to describe briefly the probability space and the statistical moments. A probability space is a triple $(\Omega, \mathcal{F}, \mathcal{P})$. Ω here is the sample space, which contains the set of all possible outcomes. $\mathcal{F}$ is the set of events, it contains all possible combinations of outcomes of Ω. In other words, $\mathcal{F}$ represents a σ-algebra of subsets of Ω. And $\mathcal{P}$ defines the probability measure on $\mathcal{F}$.

We would also like to define a random variable $\mathbf{X}$, $\mathbf{X}(\omega) : \Omega \to \mathbb{R}, \omega \in \Omega$, it is a mapping between sample space Ω and real space $\mathbb{R}$. In more general setting, the random variable $\mathbf{X}$ could map from sample space to any measurable space), the random variable could be either continuous or discrete. In order to describe the probability according to the continuous random variable, two functions are referred : the probability density function (PDF) and the cumulative distribution function (CDF).

The two basic statistical moments, expected value and variance, are the most important and common uncertainty measures. They are also referred to the first and second moment in statistics. They could be defined by using continuous and discrete random variable respectively :

$$\mathbf{E}[\mathbf{X}] = \overline{\mathbf{X}} = \int_{-\infty}^{+\infty} x f(x) dx = \sum_{i=1}^{n} x_i \rho_i \ , \tag{1}$$

$$\mathrm{Var}[\mathbf{X}] = \sigma^2(\mathbf{X}) = \int_{-\infty}^{+\infty} (x - \overline{\mathbf{X}})^2 f(x) dx = \sum_{i=1}^{n} x_i^2 \rho_i - \overline{X}^2 \ . \tag{2}$$

where, $\mathbf{X}$ is again the random variable, $f(x)$ is the probability density function according to continuous setting x. And ρ_i is the probability mass function with respect to discrete setting $x_i, i = 1, ..., n$.

2.1 Stochastic Collocation method

The Stochastic Collocation (SC) method was first introduced by Mathelin and Hussaini [14], which relies on stochastic expansion representation which relies on the Lagrange interpolating polynomials. In contrast to the non-intrusive Polynomial Chaos Expansion method, the main idea of Stochastic Collocation method is to construct Lagrange interpolation functions with known coefficients.

The collocation points and related weights are obtained by taking corresponding probability density function of each uncertain parameter into account. Stochastic and physical parameters can be easily decoupled due to the Dirac function like property of Lagrange interpolation. Still, it remains similar spectral convergence behavior like the Galerkin Polynomial Chaos method along the augmentation of polynomial's order.

We utilize first the concept of stochastic space in our numerical calculation, the stochastic space can be modelled by using the idea of multivariate statistics, therefore, it is described as :

$$\boldsymbol{\xi} = [\xi_1, \xi_2, ..., \xi_N] : \Omega \to \mathbb{R}^N \ , \tag{3}$$

where, the stochastic space has a dimensionality N. $\boldsymbol{\xi}$ is multi-index uncertain parameter representation, each of ξ_i represents a random variable with pre-defined probability distribution, e.g. normal distribution, uniform distribution, etc.

If we consider a stochastic solution $u(\boldsymbol{x}, t, \boldsymbol{\xi})$, which depends on spacial information $\boldsymbol{x}$, time t and uncertain parameters $\boldsymbol{\xi}$. The solution $u(\boldsymbol{x}, t, \boldsymbol{\xi})$ can be represented by a sum of multidimensional Lagrange polynomials :

$$u(\boldsymbol{x}, t, \boldsymbol{\xi}) = \sum_{i=0}^{\infty} \hat{u}_i(\boldsymbol{x}, t) \boldsymbol{L}_i(\boldsymbol{\xi}) \ . \tag{4}$$

In practice, the stochastic solution is approximated by truncating the summation up to certain value N_p [25], it means :

$$u(\boldsymbol{x}, t, \boldsymbol{\xi}) \approx \sum_{i=0}^{N_p} \hat{u}_i(\boldsymbol{x}, t) \boldsymbol{L}_i(\boldsymbol{\xi}) \ . \tag{5}$$

Here, N_p is actually the number of collocation points, and $\hat{u}_i(\boldsymbol{x}, t)$ is the system response of one collocation point's realization $\boldsymbol{\xi}^{(i)}$. $\boldsymbol{L}_i$ is the Lagrange interpolation polynomials, it can be constructed by using the realization points $\boldsymbol{\xi}^{(i)}$.

$$\boldsymbol{L}_i(\boldsymbol{\xi}^{(i)}) = \prod_{k=1, k\neq i}^{N_p} \frac{\boldsymbol{\xi} - \boldsymbol{\xi}^{(k)}}{\boldsymbol{\xi}^{(i)} - \boldsymbol{\xi}^{(k)}}, \quad 0 \leq i \leq N_p \ . \tag{6}$$

We could use a simple example to illustrate how the Stochastic Collocation works with Lagrange interpolating polynomials. Let's consider an ordinary differential equation (ODE) below :

$$\frac{du(x, \xi)}{dt} = -\alpha(\xi) u, \quad u(x, \xi) = \beta \ \text{ on } \ \partial D \ . \tag{7}$$

the coefficient α is uncertain parameter and depends on only one uncertain variable ξ, and β is the boundary condition. We consider α that $\alpha \backsim U(-1, 1)$, then it can be easily expressed as :

$$\alpha = \bar{\alpha} + \xi, \quad \xi \in [-1, 1] \ .$$

The solution $u(x, \xi)$ can be approximated by any arbitrary polynomial with truncation up to polynomial order N_p, then :

$$u(x, \xi) = \sum_{i=0}^{N_p} \hat{u}_i(x) \Phi_i(\xi) \ .$$

For any defined value $\xi^{(k)}$, we have :

$$u(x, \xi^{(k)}) = \sum_{i=0}^{N_p} \hat{u}_i(x) \Phi_i(\xi^{(k)}) \ .$$

Based on the expression above, regarding to one realization of ξ, the solution $u(x, \xi^{(k)})$ is still coupled with all polynomials $\Phi_i(\xi^{(k)})$. However, if we choice Lagrange polynomial $L_i(\xi)$, as $L_i(\xi^{(j)}) = \delta_{ij}$. Thence, the solution could be decoupled from each simple point of ξ due to this construction. It yields :

$$\hat{u}_i(x) \triangleq u(x, \xi^{(i)}) \ .$$

Thus, the statistical moments as we introduced at the beginning of this section can be formulated :

$$\mathbf{E}[u(x, \xi)] = \sum_{i=0}^{N_p} \hat{u}_i \int L_i(\xi) \rho(\xi) d\xi \ . \tag{8}$$

Where, $\rho(\xi)$ is the probability density function, and the quantity of the integral part from Equation (8) plays a role of a weight w_i according to each $\hat{u}_i$ for this discrete summation. However, it is not trivial to select nodes for this numerical integration, especially if the stochastic space is a multidimensional space, and the most common quadrature rules are Gaussian quadratures. Nevertheless, the number of collocation points would clearly suffer from the exponential increase due to the tensor product extension with large number of random variables.

If we denote $w_i = \int_\Omega L_i(\xi) \rho(\xi) d\xi$, the expected value and variance of the Stochastic Collocation method can be expressed like :

$$\mathbf{E}[u(x, \xi)] = \sum_{i=0}^{N_p} u(x, \xi^{(i)}) w_i \ , \tag{9}$$

$$\text{Var} = \sum_{i=0}^{N_p} u(x, \xi^{(i)})^2 w_i - \mathbf{E}[u(x, \xi)]^2 \ . \tag{10}$$

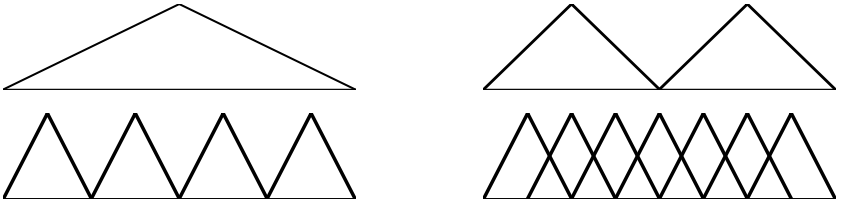

Figure 1: Piecewise linear hierarchical basis function (first 3), Lagrange like basis function (right bottom) of level 3.

2.2 Sparse grid technique

As opposed to tensor product technique [14] [23], which applies a full combination of the tensor product extension based on one dimensional quadrature points, Sparse Grid methods uses a special truncation of the tensor product expansion of a signal dimension basis for multivariate problems.

This approach was early introduced by Smolyak in 1963 [20], it was improved and generalized by Gerstner in 1998 [7]. This method constructs a quadrature rule which exploits the linear combination of tensor product, meanwhile only few points are used for the numerical integration. The main idea is that some samples produced by tensor product extension are more important than the others. By considering only those important samples with recalculated weights, and controlled by the accuracy level, the Sparse Grid techniques can increase the quality of integration and keep in low number of selected points simultaneously. In this section, we give a brief overview about this method.

The main subject of Sparse Grid techniques is to be capable of evaluating high-dimensional integrals with few quadrature points. From Uncertainty Quantification's perspective, it is about accelerating the procedure of calculating the statistical moments. If we consider the Mean calculation for a function of interest $f(\boldsymbol{\xi})$:

$$\mathbf{E}[f(\boldsymbol{\xi})] = \int_{\Omega} f(\boldsymbol{\xi})\rho(\boldsymbol{\xi})d\boldsymbol{\xi} \ . \tag{11}$$

$\rho(\boldsymbol{\xi})$ is the weighting function (or the probability density function) with multidimensional variable $\boldsymbol{\xi} = [\xi_1, \xi_2, ..., \xi_n]$, as well as for integrating domain $\Omega \subseteq \mathbb{R}^n$. As in practice, it is often the case that we do not have the analytical representation of function f, the numerical integration should be applied, i.e. numerical quadrature. As mentioned in previous Section 2.1, the Gaussian quadrature is often used for Collocation method, then the number of quadrature points will be N^d, if N is number of selected points on 1D abscissa. For the sake of simplification, we consider here only the case that the d probability distributions are identical.

Before really explaining the Sparse Grid technique, we need to first introduce the hierarchical basis function as that is what Sparse Grids depend on for approximating the uncertain parameters in stochastic spaces [15]. We will start considering the hierarchical basis function in 1D, then extend it to higher dimension.

2.2.1 1-Dimensional hierarchical basis function

Unlike the standard Lagrange basis function, Sparse Grids use the hierarchical basis, which is constructed with hat functions. The 1D hat function defines like :

$$\phi_{l,i} := \phi(2^l x - i) \ . \tag{12}$$

Where, $\phi(x) = \max(1 - |x|, 0)$, l denotes the level of the hierarchy of the basis functions, i expresses the index which locates the center point of each individual hat function (Figure 1). Similar to hierarchical basis functions in the finite element method [22] [5], we need to also introduce a hierarchical index set:

$$I_l := \{i \in \mathbb{N} : 1 \leq i \leq 2^l - 1, i \ \text{odd}\} \ . \tag{13}$$

Therefore, W_l becomes a set of hierarchical subspaces :

$$W_l := \text{span}\{\phi_{l,i}(x) : i \in I_l\} \ . \tag{14}$$

Hence, we denote V_n which is the space of piecewise linear functions on whole mesh domain :

$$V_n = \bigoplus_{l \leq n} W_l \ . \tag{15}$$

By a straightforward construction, we could approximate an arbitrary function $u(x) \in V_n$ by a unique representation :

$$u(x) = \sum_{l=1}^{n} \sum_{i \in I_l} u_{l,i} \cdot \phi_{l,i}(x) \ . \tag{16}$$

Where, $u_{l,i}$ are the coefficients which scale the corresponding basis functions $\phi_{l,i}(x)$.

2.2.2 High dimensional hierarchical basis function

Building high dimensional hierarchical basis functions, we need to apply the tensor product construction [25] [13] to combine 1D basis functions Equation (12). The d-dimensional piecewise basis functions looks like :

$$\phi_{\boldsymbol{l},\boldsymbol{i}} := \prod_{j=0}^{d} \phi_{l_j,i_j}(x_j) \ . \tag{17}$$

Note that $\boldsymbol{l}$ is multi-index representation, $\boldsymbol{l} = (l_1, ..., l_d) \in \mathbb{N}^d$, as well as for index $\boldsymbol{i}$. the definition of $\phi_{l_j,i_j}(x_j)$ is equivalent to Equation (12).

Similar to previous 1D example, the hierarchical index set become :

$$\boldsymbol{I_i} := \{\boldsymbol{i} \in \mathbb{N}^d : 1 \leq i_j \leq 2^{l_j} - 1, i_j \ \text{odd}, i \leq j \leq d\}, \tag{18}$$

the subspaces can be defined based on Equation (14) :

$$W_{\boldsymbol{l}} := \text{span}\{\phi_{\boldsymbol{l},\boldsymbol{i}}(\boldsymbol{x}) : \boldsymbol{i} \in \mathbf{I_i}\}, \tag{19}$$

the space V_n, which is supported by d-dimensional piecewise linear functions, is :

$$V_n = \bigoplus_{|\boldsymbol{l}|_\infty \leq n} W_{\boldsymbol{l}} \ . \tag{20}$$

We can again interpolate a function $u(\boldsymbol{x}) \in V_n$ by summing the d-dimensional hierarchical basis functions :

$$u(\boldsymbol{x}) = \sum_{|l|_\infty = 1}^{n} \sum_{\boldsymbol{i} \in \boldsymbol{I_i}} u_{\boldsymbol{l},\boldsymbol{i}} \phi_{\boldsymbol{l},\boldsymbol{i}}(\boldsymbol{x}) \ . \tag{21}$$

2.2.3 General construction of the Sparse Grid method

After introducing the hierarchical basis functions in high dimension, we can now discuss about the general setting of Sparse Grid (SG) method. The goal of the Sparse Grid method is trying to select the most important or effective subspaces from $W_{\boldsymbol{l}}$ to perform the numerical integration in stochastic space.

If the function $u(\boldsymbol{x})$, which we want to approximate, has a bounded mixed second derivatives [7], hence the contribution of each subspace could be determined. Based on the information of the multi-index, a Sparse Grid space can be derived :

$$\tilde{V}_n := \bigoplus_{|\boldsymbol{l}|_1 \leq n+d-1} W_{\boldsymbol{l}} \ . \tag{22}$$

For example, the Figure 2 demonstrates all the combination of 2-dimensional subspaces for a $\boldsymbol{i} \leq 5$ full grid space, and the blue squares show the selected subspaces which are suitable for constructing Spars Grids space $\tilde{V}_5$ (Equation (22)) ($|\boldsymbol{l}|_1 \leq 6$).

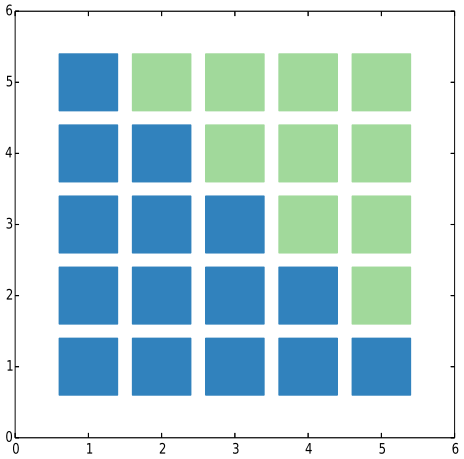

Figure 2: All squares represent the full gird space, and only blue ones represent the Sparse Grid space in the case $d = 2$, $n = 5$.

3 Head and neck FEM model deformation

3.1 Elasticity model

We employ a mechanical elasticity model to deform the region of the CTV, which should be irradiated in the therapy. Different Boundary conditions (BCs) are built from landmark displacement samples in order to calculate a displacement vector field of the whole domain. In this section, we will briefly describe the basis of the elasticity model.

In a general setting, we consider the solid domain is represented by a bounded subset $\Omega \in \mathbb{R}^3$, Γ_D and Γ_N are Dirichlet and Neumann boundary condition respectively (Figure 3), $\Gamma_D \cap \Gamma_N = \emptyset$ and $\Omega_D \cup \Omega_N = \partial\Omega$. Hence, given $\boldsymbol{f} \in L^2(\Omega)$, $\boldsymbol{g} \in L^2(\Gamma_N)$ and $\boldsymbol{u}_D \in H^1(\Gamma_D)$, we are seeking the solution $\boldsymbol{u} \in H^1(\Omega)$ in the following system :

$$-div\,\overline{\overline{\sigma}} = -\boldsymbol{f} \qquad \text{in } \Omega\,, \tag{23}$$

$$\frac{1}{2}(\nabla \boldsymbol{u} + \nabla \boldsymbol{u}^T) = \overline{\overline{\varepsilon}} \qquad \text{in } \Omega\,, \tag{24}$$

$$\overline{\overline{\sigma}} = C\overline{\overline{\varepsilon}} \qquad \text{in } \Omega\,, \tag{25}$$

$$\boldsymbol{u} = \boldsymbol{u}_D \qquad \text{on } \Gamma_D\,, \tag{26}$$

$$\overline{\overline{\sigma}}\,\boldsymbol{n} = \boldsymbol{g} \qquad \text{on } \Gamma_N\,. \tag{27}$$

Here, $\overline{\overline{\sigma}}$ is the Cauchy stress tensor, $\overline{\overline{\varepsilon}}$ is the Cauchy's train tensor, $\boldsymbol{n}$ is the normal vector on the surface Γ_N and C is the stiffness tensor (fourth order) for linear elasticity, it maps the deformation tensor $\overline{\overline{\varepsilon}}$ to stress tensor $\overline{\overline{\sigma}}$, $\overline{\overline{\sigma}}_{ij} = C_{ijkl}\overline{\overline{\varepsilon}}_{kl}$.

The explicit relationship for linear elasticity between Cauchy's stress and Cauchy's train can be written as follow :

$$\overline{\overline{\sigma}} = \lambda \mathrm{tr}(\overline{\overline{\varepsilon}})\mathbf{1} + 2\mu\overline{\overline{\varepsilon}}\,. \tag{28}$$

Where λ and μ are the Lamé coefficient for homogeneous isotropic material. In practice, the both Lamé constants would not be measured directly from experiment, they will be obtained with the help of Poisson coefficient ν and Young's modulus E :

$$\lambda = \frac{E\nu}{(1+\nu)(1-2\nu)}, \qquad \mu = \frac{E}{2(1+\nu)}\,. \tag{29}$$

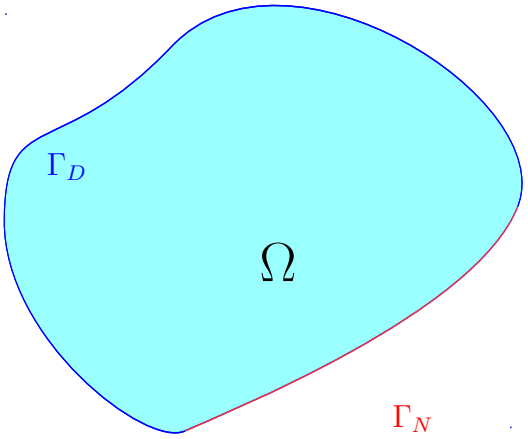

Figure 3: General setting of continuum mechanics, Ω is the solid domain, Γ_D is the Dirichlet boundary and Γ_N is the Neumann boundary.

3.2 Weak formulation

In order to approximate the solution of Equation (23), we derive the weak formulation and consider the Finite Element Method (FEM). There exist several ways to develop it, we would like to demonstrate the technique of the principle of virtual work (PVW), if we consider the virtual displacement $\delta\boldsymbol{u}$ and virtual strain tensor $\delta\boldsymbol{\varepsilon} = \frac{1}{2}(\nabla\delta\boldsymbol{u} + \nabla\delta\boldsymbol{u}^T)$.

The external virtual work yields :

$$\delta W_{ext} = \int_\Omega \boldsymbol{f}\delta\boldsymbol{u}dV + \int_{\Gamma_N} \boldsymbol{g}\delta\boldsymbol{u}dA\ . \tag{30}$$

and internal virtual work is :

$$\delta W_{int} = \int_\Omega \overline{\overline{\sigma}} : \delta\overline{\overline{\varepsilon}}dV\ . \tag{31}$$

The principle of virtual work (PVW) states that the stress, surface force and body force are in equilibrium state if and only if the external virtual work equals to the internal virtual work at every virtual displacement field [12]. The virtual displacement $\delta\boldsymbol{u}$ is arbitrary, for simplicity, we replace $\delta\boldsymbol{u}$ by v, and consider it as our test function, hence, we obtain the weak formulation for linear elasticity as follow :

$$\int_\Omega \frac{\mu}{2}(\nabla\boldsymbol{u} + \nabla\boldsymbol{u}^T)\cdot(\nabla\boldsymbol{v} + \nabla\boldsymbol{v}^T)dV + \int_\Omega \lambda(\nabla\cdot\boldsymbol{u})(\nabla\cdot\boldsymbol{v})dV = \int_\Omega \boldsymbol{f}\cdot\boldsymbol{v}dV + \int_{\Gamma_N} \boldsymbol{g}\cdot\boldsymbol{v}dA\ . \tag{32}$$

It allows us to proceed with the Finite Element Method (FEM).

3.3 The Medical Simulation Markup Language

Nowadays, patient-specific simulation became more important in biomedical modeling with the help of advanced numerical techniques. The Medical Simulation Markup Language (MSML) is a middle-ware between numerical tools in the mechanical modeling workflow for medical applications [17]. In order to achieve the patient-specific simulation, MSML divides the workflow in 5 steps : 1) contouring of the anatomy structure. 2) construction of a surface mesh based on segmented contours. 3) volumetric mesh

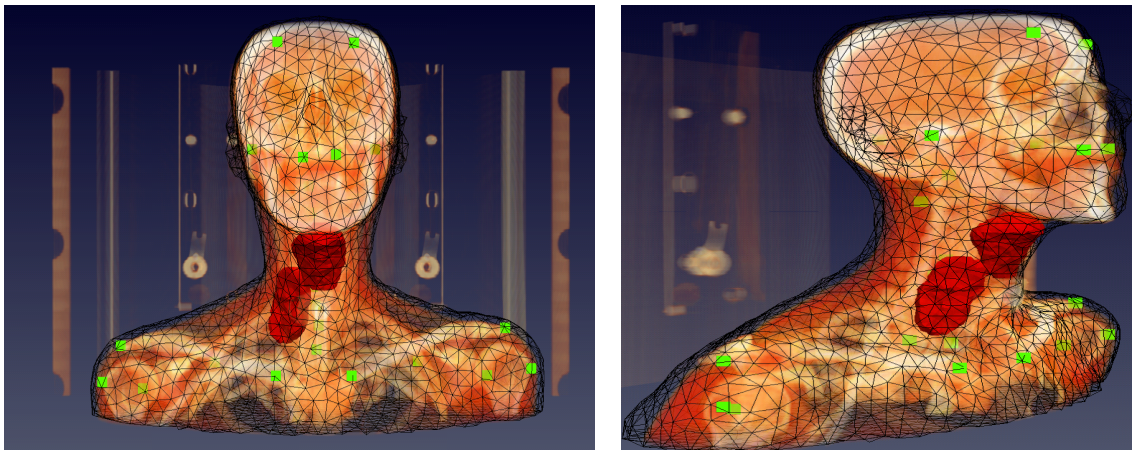

Figure 4: The finite element mesh representation with selected CTVs (red) and selected anatomical landmarks (green) on front and side

generated from surface meshes. 4) specifying biomaterial properties and boundary condition for numerical simulation. 5) post-processing of the results from numerical simulation [17]. The main role of MSML is to build a link between these 5 steps and offer an automatic process in medical engineering.

Many XML-based descriptions have been used in different physical fields [3], e.g. it is also a well suited description language for medical applications as it could represent easily typical data arising from surgical interventions and numerical simulations.

The unique feature of Medical Simulation Markup Language (MSML) is that it can operate on the full biomedical modeling process. The foundation of MSML is very generic: different descriptors could construct together the *Model description*, various descriptors can be constructed to represent a full model descriptor. Meanwhile, *Operators* are responsible for linking different data types during the workflow.

The unique feature of Medical Simulation Markup Language (MSML) is that it can operate on the full biomedical modeling process. The foundation of MSML is very generic: different descriptors could construct together the *Model description*, various descriptors can be constructed to represent a full model descriptor. Meanwhile, *Operators* are responsible for linking different data types during the workflow.

3.4 Head and neck FEM model

Biomedical finite element models can be used to simulate deformations tumor regions. We have previously generated patient specific deformable models for different patients [21] with the Medical Simulation Markup Language (MSML) [17].

In our simulation workflow a surface mesh is obtained from delineation of the skin, and the volumetric tetrahedral mesh is generated by CGAL Mesh triangulation refinement [11]. Chosen parameters for mesh generation with CGAL are facet angel = 10°, facet size = 10mm, facet distance = 5mm, cell radius edge ratio = 3 and cell size = 10mm. A linear homogeneous isotropic material [1] was chosen for the proposed biomechanical model. Based on the general solid mechanics theory (Section 3), the Young's modulus is chosen as $10MP$ and 0.4 for Poisson coefficient based on the study in [21]. Loads are applied by elastic springs forces :

$$\vec{f_i} = k \cdot \boldsymbol{d}_i, \text{ on } \Gamma_{D_l}, i = 3 \, , \tag{33}$$

which are applied between the current landmark position in the deforming model (green dots in Figure 4) and a chosen landmark target positions. $\boldsymbol{d}_i$ is the point-wise corresponding distance and k is the spring constant.

One possible use case for the model is model based deformable image registration. Landmark target positions can be extracted from fraction control image to deform the model from the patient CT image to an image from a different day with a slightly different pose of the patient. A displacement vector field

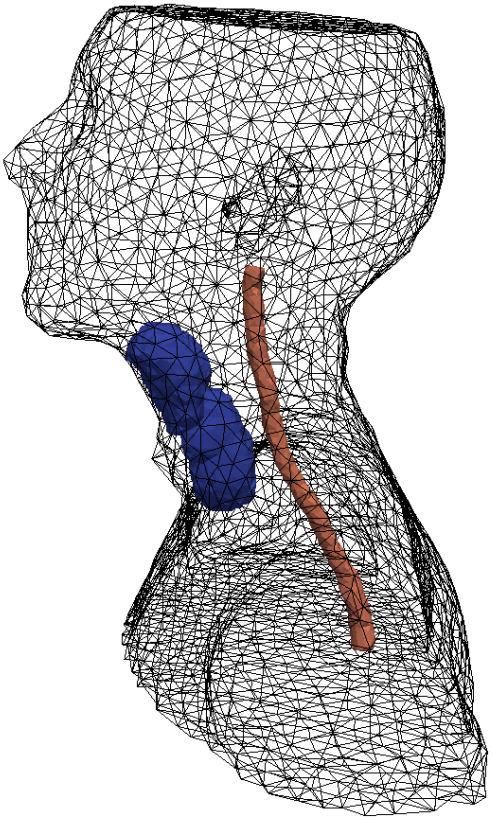

Figure 5: The physical location of CTV (blue) and the spinal cord (brown), the distance between both is used to estimate the risk to the spinal cord.

can be extracted from the simulation results, e.g. to transform delineated CTVs or OARs between the images. For instance, the numerical result can be use for estimating the risk to the spinal cord (Figure 5).

3.5 Variable margin generation with the head and neck FEM model

Yang et al. [26] introduced a method based on individual landmark position uncertainties to calculate a variable margin using the landmark displacement information from a patient cohort. The local margin size is computed as a weighted average of the expected displacements of near landmarks.

We previously improved Yang's approach and considered the landmarks displacements are dependent and combine them into a single reducible feature vector: A pose $\boldsymbol{u}(f)$ [21]. The main idea is to use a probabilistic principle component analysis (PPCA) [10] [24] in order to obtain the first five eigenvectors $b_1, ..., b_5$ from a large number of different poses from different patients and different therapy fraction. Each pose $\boldsymbol{u}(f)$ on a fraction f can then be approximated with a linear combination of the first five eigenvectors:

$$\boldsymbol{u}(f) \approx [b_1, ..., b_5]^T \cdot [q_1, ..., q_5] + \bar{\boldsymbol{u}} \ , \tag{34}$$

where $q_1, ..., q_5$ are the coefficients for the pose. We proposed to generate $N = 400$ random samples for the previous coefficients $(q_1, ..., q_5)$ to generate pose scenarios before the treatment. Each pose scenario builds loads for a simulation using the FEM model (section 3.4) . The resulting displacement vector filed can be used to transform the CTV to each scenario and a margin is extracted by accumulating the transformed CTV. More details can be found in [21].

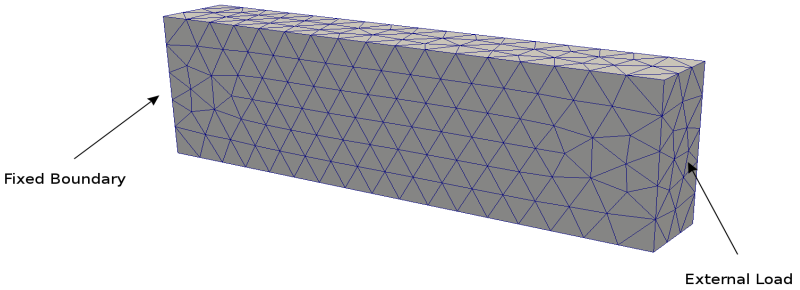

Figure 6: 3D elasticity beam, left side is considered as fixed and right side is charged by an external load.

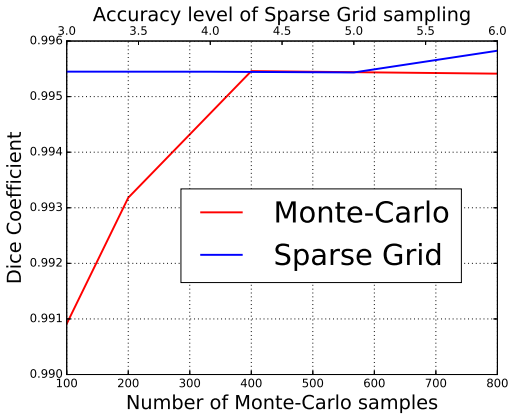

Figure 7: Comparison of Dice coefficient between the reference solution and both sampling methods.

Accuracy level	3	4	5	6
Number of samples	3	4	5	6

Table 1: Number of Sparse Grid samples with correspoing accuracy level in 1D.

4 Implementation of the Sparse-Grid method

We added Sparse Grid sampling methods to the MSML in order to allow uncertainty analysis for biomechanical models.

4.1 Validation of the implementation

Before utilizing our implementation of the Sparse Grid sampling method in our biomechanical simulation, we need to verify it with simple test cases that allow us to calculate analytically a reference solution. Therefore, we will show how Sparse Grid method could reduce number of sampling points compared to Monte-Carlo methods. Elasticity beam models will be used as a testing model.

4.1.1 Model with one random variable

First we use a 3D elasticity beam with a fixed boundary on the left side and a horizontal external load on the right side as a testing case (see Figure 6).

We apply therefore the general solid mechanics model (Equation (23)) with a Dirichlet boundary condition on the left of the beam (Equation (26)) and a Neumann boundary condition on the right (Equation (27)). For the sake of the simplicity, we set the Poisson coefficient ν to zero. It would facilitate the comparison between two sampling methods, because as result, the elastic beam will only deform along

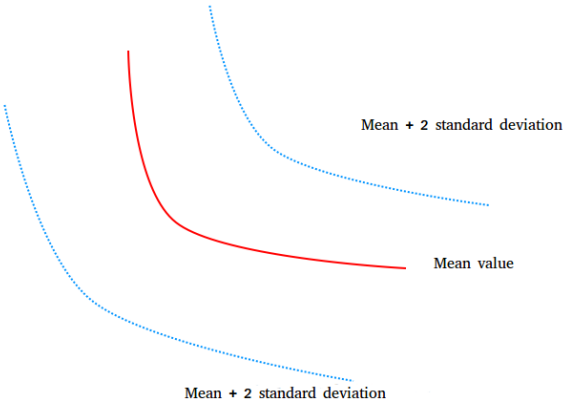

Figure 8: 2D illustration of the measured volume. Red line represents the iso-surface of mean value, and two blue lines represent the iso-surface of $mean \pm 2\sigma$. The volume between two blue lines.

horizontal direction, and we could analytically create a reference result.

In this case, we consider the external force as an uncertain source, which has normal distribution behavior with a mean value as 1.0 N and standard deviation 0.01. We measure the volume between two iso-surfaces (see Figure 8), which are defined by $\pm 2\sigma$ (2 blue dash lines) with respect to the mean surface (red line). Figure 10 demonstrates the inner iso-surface and outer iso-surface of tumor volume after simulation. Thence, we could compute the dice coefficient [6] between numerical results and a analytical solution. We therefore consider 4 different Monte-Carlo sample sets, which include 100, 200, 400, and 800 samples respectively, and also 4 levels of accuracy from 3 to 6 with Sparse Grid sampling.

The comparison (Figure 7) shows that Sparse Grid achieves from very beginning with only 3 sample points above 0.995 Dice coefficient. In contrast, Monte-Carlo only obtains 0.990 with 100 samples. Meanwhile, the Dice coefficient of Sparse Grid increases while we raise the level of accuracy, it corresponds well the theorem of the Collocation method as it is polynomial based. At same time, Monte-Carlo method's result has a small reduction at 400 samples, it is also a good indicator as Monte-Carlo method has a "oscillatory" behavior in convergence.

We have to admit that in this single random variable example, Monte-Carlo method offers also a very good result even with only 100 samples, the difference of the Dice coefficient between Sparse Grid level 3 and Monte-Carlo 100 samples is only 0.5%. Both methods could converge very quickly, as this "1D" case is indeed simplified. For the Monte-Carlo sampling, the random points are re-sampled at each simulation (with fixed number of samples), we could meantime reuse of course the old sampling and adding new random points for higher number of samples, it would reduce the oscillatory" behavior, but for real clinical situation, it is not often the case.

4.1.2 Model with two random variables

After comparing the signal random variable elastic beam, we created a second example with two random input resources. We consider again the same geometry as in Section 4.1.1. This time, instead of applying one external force on the right side, we charge both sides with random external forces. We hence move the fixed boundary condition (Figure 6) to the middle of the beam (Figure 9). This condition is actually no longer a boundary condition, we replace this constraint to the middle of the object in order to have an unmovable center point, it could simplify the following comparison.

Again, we artificially set the Poisson coefficient ν to zero, the deformation will consequently only happen along horizontal direction with a fixed center point. In this case, the number of sampling points for Sparse Grid increases very fast with the level of accuracy due to the exponential nature (Table 2), e.g. 89 sample points instead of 6 for level 6 in single random variable case. However, Sparse Grid method has again even better result than previous case (in Section 4.1.1), the difference of Dice coefficient increases,

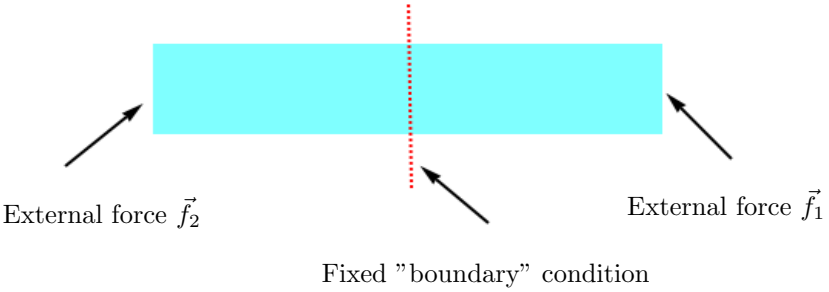

Figure 9: Cross section of 3D beam, with 2 external forces and one middle fixed "boundary" condition.

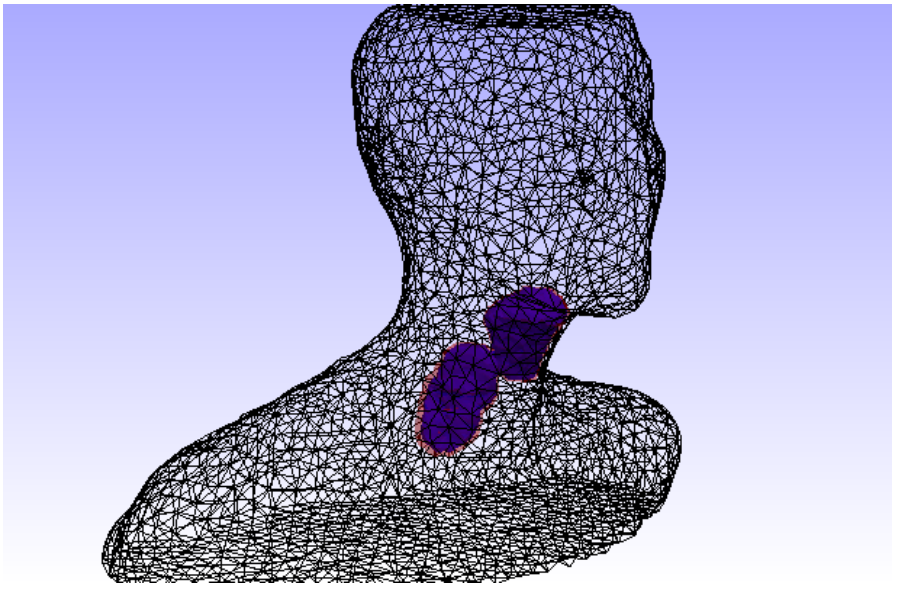

Figure 10: Inner iso-surface (blue) and outer iso-surface (red).

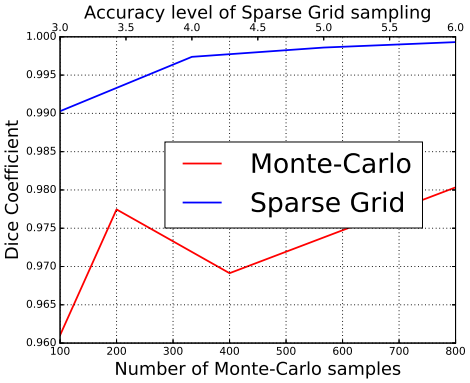

Figure 11: Comparison of Dice coefficient between the reference solution and both sampling methods.

Accuracy level	3	4	5	6
Number of samples	13	29	53	89

Table 2: Number of Sparse Grid samples with correspoing accuracy level in 2D.

Accuracy level	1	2	3
Number of samples	11	61	241
Dice coefficient	0.988234	0.988279	0.988376

Table 3: Number of Sparse Grid samples with correspoing accuracy level in for Head and Neck simulation.

and Monte-Carlo method shows the similar behavior from the earlier example.

We have to mention that the number of sampling points for Sparse Grid method increases very quick when we increase the level of accuracy, if the dimension of random variable is large. We want to clarify that in the framework of the Medical Simulation Markup Language, it is still meaningful to have the viability of using an importance sampling technique as there are still massive medical applications which consider limited numbers of random variables.

4.2 Evaluation of Sparse-Grid in Head and Neck model

We propose to use the Sparse Grid method instead of Monte-Carlo sampling of for the coefficients $(q_1, ..., q_5)$ during the margin calculation (Section 3.5) the Variable margin generation. We expect to save computation effort due to a reduction of the number of required simulations with the head and neck FEM model.

As we cannot easily obtain a analytical reference solution, we created a reference solution by running a large number of simulations using the Monte-Carlo method. Hence, we processed 20 Monte-Carlo simulations, each of them included 2000 random samples, and the final reference data is selected by the best solution by doing cross comparison within those 20 results.

We accomplished therefore a similar comparison as in Section 4. We compared the Sparse Grid method from accuracy level 1 to 3 against a Monte-Carlo sampling sets with samples from 100 to 800 (which is twice number of samples proposed in [21].

We use the Dice coefficient again as an indicator in order to evaluate the results. We can see even with small number of samples from Sparse Grid method, the quality of our numerical result performances always better than Monte-Carlo sampling.

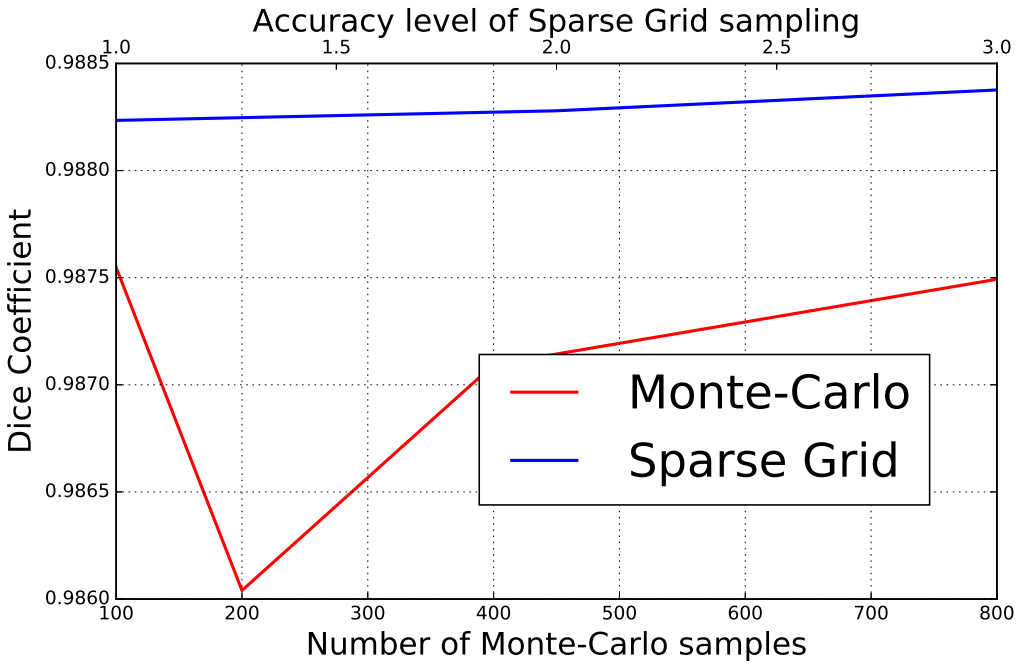

Figure 12: Comparison of Dice coefficient between the reference solution and both sampling methods.

5 Conclusions

We implemented a Sparse Grid sampling method in Medical Simulation Markup Language (MSML) framework, it offers a new way to simplify the process of quantifying the uncertainties when we have randomness in the inputs of our numerical simulation, especially for Head and Neck tumor margin generation. We first compare in Section 4 Sparse Grids with a Monte-Carlo method by using two examples in order to observe the convergence behavior of these two methods. And we studied again these two different sampling strategies for a real Head and Neck tumor margin quantification simulation, it shows once more that Spars Grids have a better convergence rate. We should be aware that Sparse Grids have a very good performance in term of cost if the number of random variable is considerable small, in contrast, the Sparse Grid method is not cheap anymore if we want to have the exponential convergence, but for our specific case, Head and Neck tumor margin generation, the number of uncertain parameter is rather small ($n = 5$), we can therefore still benefit from Sparse Grid technique. We should also mention, in our studies, the samples of Monte-Carlo method is rather small (max. 800), it is not very representative for Monte-Carlo sampling, but in our medical application only 400 samples are reasonable [21], that is the reason we keep a low range number of Monte-Carlo for comparison.

References

[1] Jérémie Allard, Stéphane Cotin, François Faure, Pierre-Jean Bensoussan, François Poyer, Christian Duriez, Hervé Delingette, and Laurent Grisoni. SOFA - an Open Source Framework for Medical Simulation. In *MMVR 15 - Medicine Meets Virtual Reality*, volume 125 of *Studies in Health Technology and Informatics*, pages 13–18, Palm Beach, United States, February 2007. IOP Press.

[2] R Bendl, J Pross, A Hoess, M Keller, K Preiser, and W Schlegel. VIRTUOS - a program for virtual radiotherapy simulation and verification. *Proc 11th International Conference on the use of Computers in Radiation Therapy, Manchester/UK*, 3:226–227, 1994.

[3] R. Carey and G. Bell. *The Annotated VRML 2.0 Reference Manual*. A-W Developers Press Series. Addison-Wesley Developers Press, 1997.

[4] Allen M. Chen, D. Gregory Farwell, Quang Luu, Paul J. Donald, Julian Perks, and James A. Purdy. Evaluation of the planning target volume in the treatment of head and neck cancer with intensity-modulated radiotherapy: What is the appropriate expansion margin in the setting of daily image guidance? *International Journal of Radiation Oncology Biology Physics*, 81(4):943–949, 2011.

[5] Saikat Dey, Mark S. Shephard, and Joseph E. Flaherty. Symposium on advances in computational mechanics geometry representation issues associated with p-version finite element computations. *Computer Methods in Applied Mechanics and Engineering*, 150(1):39 – 55, 1997.

[6] Lee R. Dice. Measures of the amount of ecologic association between species. *Ecology*, 26(3):297–302, 1945.

[7] Thomas Gerstner and Michael Griebel. Numerical integration using sparse grids. *Numerical Algorithms*, 18(3):209–232, 1998.

[8] T Gupta and CAnand Narayan. Image-guided radiation therapy: Physician's perspectives. *Journal of Medical Physics*, 37(4):174, oct 2012.

[9] Serhat Hosder, Robert W Walters, and Rafael Perez. A non-intrusive polynomial chaos method for uncertainty propagation in cfd simulations. *AIAA paper*, 891:2006, 2006.

[10] J.E. Jackson. *A User's Guide to Principal Components*. Wiley Series in Probability and Statistics. Wiley, 2005.

[11] Clément Jamin, Pierre Alliez, Mariette Yvinec, and Jean-Daniel Boissonnat. CGALmesh: a Generic Framework for Delaunay Mesh Generation. *ACM Transactions on Mathematical Software*, 41(4):24, October 2015.

[12] C. Lanczos. *The Variational Principles of Mechanics*. Dover Books On Physics. Dover Publications, 1970.

[13] Olivier Le Maître and Omar M Knio. *Spectral methods for uncertainty quantification: with applications to computational fluid dynamics*. Springer Science & Business Media, 2010.

[14] Lionel Mathelin and M. Yousuff Hussaini. A stochastic collocation algorithm for uncertainty analysis. *NASA*, pages 2003–212153, 2003.

[15] Dirk Pflueger, Benjamin Peherstorfer, and Hans-Joachim Bungartz. Spatially adaptive sparse grids for high-dimensional data-driven problems. *Journal of Complexity*, 26(5):508 – 522, 2010.

[16] Matthew T. Reagan, Habib N. Najm, Roger G. Ghanem, and Omar M. Knio. Uncertainty quantification in reacting-flow simulations through non-intrusive spectral projection. *Combustion and Flame*, 132(3):545 – 555, 2003.

[17] Suwelack S, Stoll M, Schalck S, Schoch N, Dillmann R, Bendl R, Heuveline V, and Speidel S. The medical simulation markup language-simplifying the biomechanical modeling workflow. *Medicine Meets Virtual Reality 21: NextMed/MMVR21*, 196:394, 2014.

[18] A Saunders, W B Guminski, and Coman A D. Cancer of the Head and Neck. In Elizabeth C. Ward and Corina J. van As-Brooks, editors, *Head and Neck Cancer: Treatment, Rehabilitation, and Outcomes*. Plural Publishing, 2014.

[19] Wolfgang Schlegel, Otto Pastyr, Thomas Bortfeld, Gerd Becker, Lothar Schad, G??nther Gademann, and Walter J. Lorenz. Computer systems and mechanical tools for stereotactically guided conformation therapy with linear accelerators. *International Journal of Radiation Oncology, Biology, Physics*, 24(4):781–787, 1992.

[20] S. A. Smolyak. Quadrature and interpolation formulas for tensor products of certain classes of functions. 1963.

[21] Markus Stoll, Eva Maria Stoiber, Sarah Grimm, Jürgen Debus, Rolf Bendl, and Kristina Giske. Comparison of Safety Margin Generation Concepts in Image Guided Radiotherapy to Account for Daily Head and Neck Pose Variations. *PLoS ONE*, 11(12):e0168916, 2016.

[22] B.A. Szabo and I. Babuška. *Finite Element Analysis*. A Wiley-Interscience publication. Wiley, 1991.

[23] Menner A. Tatang, Wenwei Pan, Ronald G. Prinn, and Gregory J. McRae. An efficient method for parametric uncertainty analysis of numerical geophysical models. *Journal of Geophysical Research: Atmospheres*, 102(D18):21925–21932, 1997.

[24] Michael E. Tipping and Chris M. Bishop. Probabilistic principal component analysis. *Journal of the Royal Statistical Society, Series B*, 61:611–622, 1999.

[25] Dongbin Xiu. *Numerical methods for stochastic computations: a spectral method approach.* Princeton University Press, 2010.

[26] Jinzhong Yang, Adam S. Garden, Yongbin Zhang, Lifei Zhang, and Lei Dong. Variable planning margin approach to account for locoregional variations in setup uncertaintiesa). *Medical Physics*, 39(8):5136–5144, 2012.

Preprint Series of the Engineering Mathematics and Computing Lab

recent issues

No. 2016-02 Jonas Kratzke, Vincent Heuveline: An analytically solvable benchmark problem for fluid-structure interaction with uncertain parameters

No. 2016-01 Philipp Gerstner, Michael Schick, Vincent Heuveline, Nico Meyer-Hübner, Michael Suriyah, Thomas Leibfried, Viktor Slednev, Wolf Fichtner, Valentin Bertsch: A Domain Decomposition Approach for Solving Dynamic Optimal Power Flow Problems in Parallel with Application to the German Transmission Grid

No. 2015-04 Philipp Gerstner, Vincent Heuveline, Michael Schick : A Multilevel Domain Decomposition approach for solving time constrained Optimal Power Flow problems

No. 2015-03 Martin Wlotzka, Vincent Heuveline: Block-asynchronous and Jacobi smoothers for a multigrid solver on GPU-accelerated HPC clusters

No. 2015-02 Nicolai Schoch, Fabian Kißler, Markus Stoll, Sandy Engelhardt, Raffaele de Simone, Ivo Wolf, Rolf Bendl, Vincent Heuveline: Comprehensive Pre- & Post-Processing for Numerical Simulations in Cardiac Surgery Assistance

No. 2015-01 Teresa Beck, Martin Baumann, Leonhard Scheck, Vincent Heuveline, Sarah Jones: Comparison of mesh-adaptation criteria for an idealized tropical cyclone problem

No. 2014-02 Christoph Paulus, Stefan Suwelack, Nicolai Schoch, Stefanie Speidel, Rüdiger Dillmann, Vincent Heuveline: Simulation of Complex Cuts in Soft Tissue with the Extended Finite Element Method (X-FEM)

No. 2014-01 Martin Wlotzka, Vincent Heuveline: A parallel solution scheme for multiphysics evolution problems using OpenPALM

No. 2013-04 Nicolai Schoch, Stefan Suwelack, Stefanie Speidel, Rüediger Dillmann, Vincent Heuveline: Simulation of Surgical Cutting in Soft Tissue using the Extended Finite Element Method (X-FEM)

No. 2013-03 Martin Wlotzka, Edwin Haas, Philipp Kraft, Vincent Heuveline, Steffen Klatt, David Kraus, Klaus Butterbach-Bahl, Lutz Breuer: Dynamic Simulation of Land Management Effects on Soil N2O Emissions using a coupled Hydrology-Ecosystem Model

No. 2013-02 Martin Baumann, Jochen Förstner, Bernhard Vogel, Vincent Heuveline, Jonas Kratzke, Sebastian Ritterbusch, Heike Vogel: Model-based Visualization of Instationary Geo-Data with Application to Volcano Ash Data

No. 2013-01 Martin Schindewolf, Björn Rocker, Wolfgang Karl, Vincent Heuveline: Evaluation of two Formulations of the Conjugate Gradients Method with Transactional Memory

No. 2012-07 Andreas Helfrich-Schkarbanenko, Vincent Heuveline, Roman Reiner, Sebastian Ritterbusch: Bandwidth-Efficient Parallel Visualization for Mobile Devices

No. 2012-06 Thomas Henn, Vincent Heuveline, Mathias J. Krause, Sebastian Ritterbusch: Aortic Coarctation simulation based on the Lattice Boltzmann method: benchmark results

Preprint Series of the Engineering Mathematics and Computing Lab (EMCL)

http://emcl.iwr.uni-heidelberg.de